Infrared Physics Vol. 22, pp. 9 to 22, 1982
Printed in Great Britain

0020-0891/82/010009-14$03.00/0
Pergamon Press Ltd

Reprinted a
in "Infrare
Design", edi
by R.B. Johnso
and W.L. Wolfe
1983.

TWO-DIMENSIONAL EFFECTS IN INTRINSIC PHOTOCONDUCTIVE INFRARED DETECTORS

A. KOLODNY and I. KIDRON

Microelectronics Research Center, Department of Electrical Engineering, Technion-Israel Institute of Technology, Haifa 32000, Israel

(*Received* 17 *June* 1981)

Abstract—Two-dimensional effects on the current responsivity and response time of intrinsic quantum photoconductive infrared detectors are presented in detail. Deviations from first-order theory are shown to be pronounced for the case of devices of small optically sensitive area with planar electrodes. Expressions are derived that lend themselves to numerical calculations. Specific results are given for $Hg_{1-x}Cd_xTe$ detectors of various geometries and operating conditions. A novel structure for a photoconductive detector array with asymmetric contacts is proposed and analysed.

INTRODUCTION

Intrinsic photoconductive semiconductor infrared detectors are widely used in passive thermal imaging and tracking systems. The theory of responsivity, speed of response and noise in these devices is given in the literature, based on one-dimensional models.[1–10] In order to meet the spatial resolution requirements of modern systems (of the order of 0.1 mrad) there is a trend to minimize the dimensions of the detectors for a given optical aperture. Typically, the device length and width are of the order of 25 μm, and the semiconductor thickness is 10–15 μm. The optically active length is determined by the spacing between planar metal contacts placed on the upper semiconductor surface. Due to the location of the contacts and since the length and thickness of the photodetector are of the same order of magnitude, two-dimensional effects must be considered. Indeed, measurements on such devices reveal that responsivity does not exactly follow the one-dimensional theory.[10] Deviations from simple theory are also found in the speed of response of small detectors, a parameter of particular importance in serially-scanned systems with bandwidths of the order of 10 MHz. Transit-time considerations predict a response time of about $L/2v$, where v is the carrier drift velocity and L is the element length; in actual practice one measures longer times, which may be due to blocking contacts[10] and, as will be shown, due to two-dimensional ambipolar trajectories of the excess carriers in the device.

In this paper we present a two-dimensional analysis of photoconductor responsivity, taking into account the device geometry, the non-uniform electric field and the boundary conditions. Numerical simulation results are given to demonstrate the effects of planar contacts and minority carrier blocking at the contact in a two-dimensional structure. The effect of asymmetric electrodes on spatial sensitivity is also investigated. Two-dimensional effects on the speed of response are discussed using an heuristic approach and compared to experimental results.

ANALYSIS

The current responsivity of a photoconductive detector is defined as the ratio of optically-induced change in terminal current to the optical power incident upon the device, when it is biased to a constant voltage. This current change is caused by the optically generated excess carrier distribution in the entire device volume. To find the responsivity, one must first determine the excess carrier distribution for a given optical excitation. Under low-level illumination, the excess carrier density may be found by solving the ambipolar transport problem.[1,11] For an n-type semiconductor, assuming

quasi-neutrality and neglecting trapping, the governing equation is

$$\frac{\partial \hat{p}}{\partial t} = \frac{\hat{p}}{\tau_a} + g_{\text{opt}} + D_a \nabla^2 \hat{p} - \mu_a \mathbf{E} \cdot \nabla \hat{p}. \tag{1}$$

In equation (1) $\hat{p}$ is the excess carrier density, D_a, μ_a and τ_a are the ambipolar diffusion constant, mobility and lifetime (which approach the minority carrier parameters D_p, μ_p and τ_p, for an extrinsic semiconductor); g_{opt} is the optical generation rate. The electric field $\mathbf{E}$ in equation (1) may be approximated by the field in the non-illuminated case $\mathbf{E}_0$, neglecting the internal field $\hat{E}$ associated with the carrier distributions. This approximation leads to a second-order inaccuracy in $\hat{p}$.[1,11] However, $\hat{E}$ contributes a first-order term to the current density $\mathbf{j}$ at any point in the device:

$$\mathbf{j} = \mathbf{j}_0 + \hat{j} = q(\mathbf{E}_0 + \hat{E})[(\bar{n} + \hat{n})\mu_n + (\bar{p} + \hat{p})\mu_p] + q(D_n \nabla \hat{n} - D_p \nabla \hat{p}). \tag{2}$$

Here, $\mathbf{j}_0$ is the current density in the non-illuminated case and $\hat{j}$ is current density due to the photocarriers. Given the solution of equation (1) with prescribed boundary conditions and optical excitation, we proceed with the derivation of current responsivity of the detector. Our goal is to find the change in terminal current $\hat{I}$ caused by the illumination and eliminate $\hat{E}$ by means of integrations, extending the approach outlined by Rittner.[1] Subtracting the terms representing $\mathbf{j}_0$ from the right-hand side of equation (2) and integrating along any flowline l between the two contacts we obtain

$$\int_l \hat{j} \cdot \mathrm{d}\mathbf{l} = q(\mu_n + \mu_p)\left[\int_l \hat{p}\mathbf{E}_0 \cdot \mathrm{d}\mathbf{l} + \int_l \hat{p}\hat{E} \cdot \mathrm{d}\mathbf{l}\right]. \tag{3}$$

The integral of the diffusion terms vanishes since the excess carrier density is zero at the two ohmic contacts; the integral $\int_l \hat{E} \cdot \mathrm{d}\mathbf{l}$ must vanish since a constant voltage is applied across the device. The term $\int_l \hat{p}\hat{E} \cdot \mathrm{d}\mathbf{l}$ in equation (3) is nonzero, but is negligible under low-level illumination. We now assume that the direction of field lines does not change significantly by the low-level illumination, since $|\mathbf{E}_0| \gg |\hat{E}|$. Thus, the direction of dl coincides with the direction of $\mathbf{E}_0$, and equation (3) becomes

$$\int_l |\hat{j}|\, \mathrm{d}l = q(\mu_n + \mu_p) \int_l \hat{p}\, |\mathbf{E}_0|\, \mathrm{d}l. \tag{4}$$

We now divide both sides of equation (4) by the length of the integration path, and perform additional integration over the entire volume of the device. Using spatial coordinates j and k which are orthogonal to the flow lines, we get

$$\iiint \frac{|\hat{j}|\, \mathrm{d}l\, \mathrm{d}k\, \mathrm{d}j}{l} = q(\mu_n + \mu_p) \iiint \frac{\hat{p}\, |\mathbf{E}_0|}{l}\, \mathrm{d}l\, \mathrm{d}k\, \mathrm{d}j. \tag{5}$$

The expression on the right-hand side is the integral of $\hat{p}\,|E_0|/l$ over the total device volume. On the left-hand side we can write $\mathrm{d}\hat{I} = |\hat{j}|\, \mathrm{d}k\, \mathrm{d}j$, where $\mathrm{d}\hat{I}$ is the differential of the response current, so that

$$\int_{\text{all flow lines}} \int_l \frac{\mathrm{d}I\, \mathrm{d}l}{l} = \int_v \frac{\hat{p}\, |\mathbf{E}_0|}{l}\, \mathrm{d}v. \tag{6}$$

Since $\mathrm{d}I$ is constant along the flow line, the length l is integrated out, and we obtain the final expression for the change in terminal current caused by illumination:

$$\hat{I} = \int_{\text{all flow lines}} \mathrm{d}I = \int_v \frac{\hat{p}\, |\hat{E}_0|}{l}\, \mathrm{d}v. \tag{7}$$

In a two-dimensional analysis we can use Cartesian coordinates and assume that there are no changes along the z-axis. See Fig. 1. The calculation per unit z may be performed on a cross section in the x–y plane, and equation (7) is rewritten as

$$\hat{I} = \iint \frac{\hat{p}(x, y)\,|E_0(x, y)|}{l(x, y)}\,\mathrm{d}x\,\mathrm{d}y, \tag{8}$$

where $\hat{p}(x, y)$ is the excess carrier density at point (x, y), $|E_0(x, y)|$ is the electric field intensity at that point, and $l(x, y)$ is the length of the flow line passing through this point.

Note that if the field magnitude is constant throughout the device, equation (8) reduces to the familiar one-dimensional expression

$$\hat{I} = q(\mu_n + \mu_p)(V/L^2)\hat{P}, \tag{9}$$

where $\hat{P}$ is the total number of excess carriers in the entire device volume, L is the uniform length of flow lines, and the field is equal to the bias voltage V divided by L. The essential feature of a one-dimensional model is that the response current does not depend on the detailed excess carrier distribution, but rather on their total amount. However, in a practical detector, which is two-dimensional in nature, the contribution of excess carriers at each point to the photocurrent depends upon the electric field magnitude and the length of the flow line traversing this point. The differences in the contribution of various regions to the responsivity are pronounced by the fact that flow lines are shorter at points where the field intensity is higher.

The responsivity calculation described above has been implemented in two-dimensional numerical computer programs. Figure 1 illustrates a typical problem. The first computational step is to find the normalized electric potential distribution $\phi(x, y)$ in a cross section of the device, by solving Laplace's equation (as mentioned earlier, we neglect the perturbation in electric field due to photocarriers). This step is performed once for each device geometry, using as boundary conditions a prescribed applied voltage across the equipotential electrodes. The electric field is obtained by taking the numerical gradient of the potential.

In the second step, the excess carrier distribution is found from numerical solution of the ambipolar equation (with minority carrier parameters)

$$D_p\left(\frac{\partial^2\hat{p}}{\partial x^2} + \frac{\partial^2\hat{p}}{\partial y^2}\right) + \mu_p E_x\frac{\partial\hat{p}}{\partial x} + \mu_p E_y\frac{\partial\hat{p}}{\partial y} - \frac{\hat{p}}{\tau_p} = -g_{\mathrm{opt}}(x, y), \tag{10}$$

where E_x and E_y are the previously calculated components of the potential gradient. The

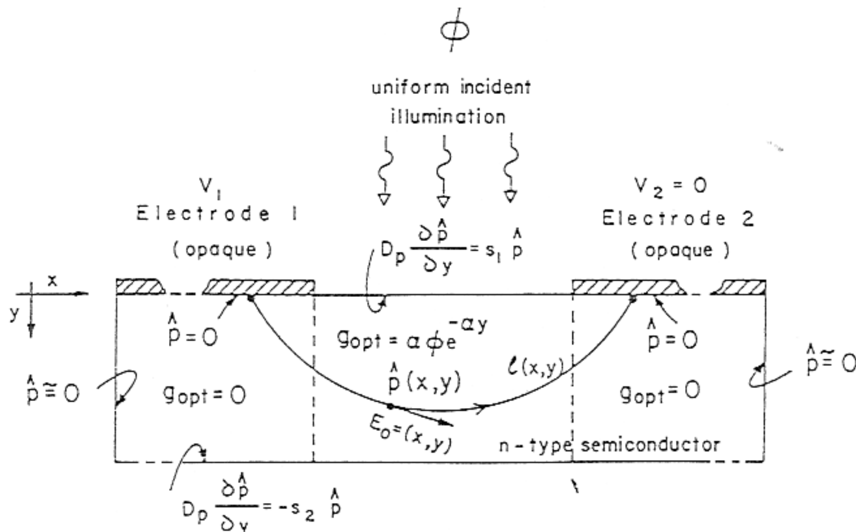

Fig. 1. Illustration of geometry and boundary conditions for a cross-section of a photoconductive detector with planar electrodes.

optical generation takes place under the exposed part of the semiconductor surface, and its dependence on photon flux density $\phi(x)$, absorption coefficient α and depth y is

$$g_{opt}(x, y) = \alpha\phi(x)e^{-\alpha y}. \tag{11}$$

Boundary conditions for equation (10) include surface recombination at the non-metallized interfaces

$$D_p \frac{\partial \hat{p}}{\partial \mathrm{n}} = s\hat{p}, \tag{12}$$

where n is the normal to the surface. The surface recombination velocity s is an effective value, affected by the existence of surface fields induced by interface charges in passivation layers.[12] The surface space-charge layer is neglected in our calculation. An accumulation layer may be modeled by a short conductance which does not affect current responsivity (although it lowers the voltage responsivity). For metal-semiconductor ohmic contacts, the boundary condition is $\hat{p} = 0$. If there is a built-in retarding field for minority-carriers due to high n^+ doping near the electrode,[2,13] the contact may be regarded as ideally blocking, so that

$$\mu_p \mathrm{E}_n \hat{p} = D_p \frac{\partial \hat{p}}{\mathrm{dn}}, \tag{13}$$

where E_n is the field normal to the contact. The solution of equation (10) is repeated for various field strengths and parameter values, giving the excess carrier distribution for each case.

The third step in the computation of responsivity is the determination of the length of the flow line passing through each point in the device cross-section. The flow lines (field lines) are orthogonal to the equi-potential lines, and are easily obtained as the contours of the stream-function $\psi(x, y)$. This function is the harmonic conjugate of the potential $\phi(x, y)$, found by solving Laplace's equation again using conjugate boundary conditions. Contour lengths are found for several values of ψ, and are mapped to all $\psi(x, y)$ by interpolation.

Finally, the detector responsivity is found by evaluating the integral of equation (8) and dividing by the optical power of the incident photon flux.

PLANAR-CONTACT PHOTOCONDUCTORS

The above analysis is used to investigate in detail the characteristics of photoconductors. Figure 2 shows the potential, excess carrier density and stream function for a detector with planar non-blocking contacts. The simulation parameters correspond to an n-type $Hg_{0.795}Cd_{0.205}Te$ semiconductor at 77K, exposed to a uniform monochromatic photon flux at 10 μm wavelength. The device is operated at a bias voltage of 50 mV, which makes the excess carrier distribution skewed towards the left contact. It is evident from Fig. 2 that most of the photoresponse comes from the upper region in the exposed area, due to the high excess carrier density, the high electric field, and the short flow lines, relative to other regions. The responsivity is very sensitive to the recombination velocity at the front surface. For the example of Fig. 2, the responsivity calculated by equation (8) is $452\ \mathrm{A \cdot W^{-1}}$.

Figure 3 shows the effect of varying the bias voltage on excess carrier distribution in an n-type photoconductive detector with planar non-blocking contacts. The surface recombination velocity is assumed to be zero. At low bias the distribution is determined by the high absorption near the upper surface, and by diffusion towards the bulk and the two contacts, where recombination takes place (Fig. 3a). As the bias is increased, the electric field tends to draw the excess carriers towards the negative electrode, and the total amount of excess carriers in the device decreases due to enhanced recombination at the collecting electrode (Fig. 3d). This sweepout of excess carriers limits the responsivity at high electric fields. Two-dimensional calculation of responsivity vs bias lead to characteristics similar to those derived by Rittner[1] for a one-dimensional device. A comparison is

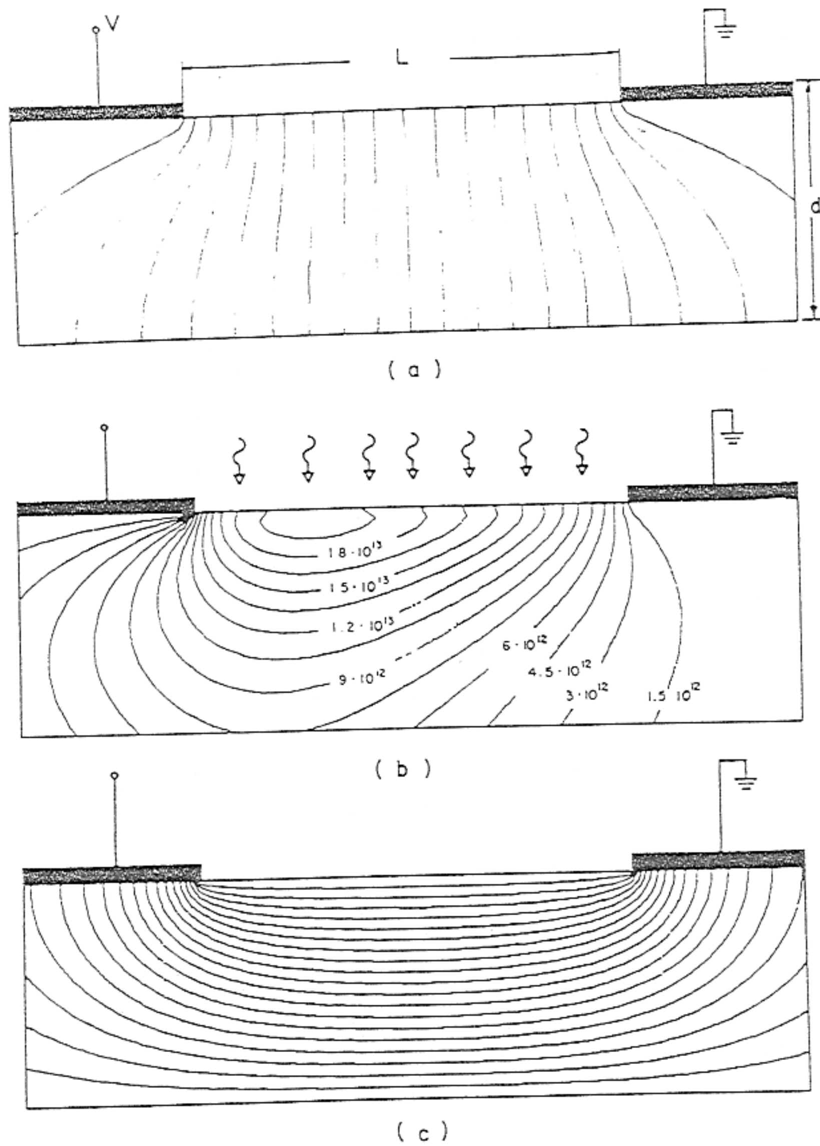

Fig. 2. (a) Equipotential lines in a cross-section of a planar-contact photoconductor. (b) Equiconcentration contours (in cm^{-3}), showing the excess-carrier density distribution in the device under uniform illumination. (c) Flow lines map. The simulated device is n-type $Hg_{0.795}Cd_{0.205}Te$ at 77K, uniformity illuminated by a photon flux density $\phi = 10^{17}\ cm^{-2}\cdot s^{-1}$ at wavelength $\lambda = 10\ \mu m$. The optically active length is $L = 28\ \mu m$, the thickness is $d = 15\ \mu m$, and the absorption depth is $\alpha^{-1} = 1.25\ \mu m$. The hole mobility is $\mu_p = 500\ cm^2\cdot V^{-1}\cdot s^{-1}$, and the lifetime $\tau_p = 3 \times 10^{-6}$ s. Surface recombination velocity $s = 2 \times 10^3\ cm\cdot s^{-1}$ is assumed at the front and rear surfaces. Operating bias is $V = -50$ mV.

given in Fig. 4, which shows the ratio of responsivities calculated by two-dimensional and one-dimensional models (for the same detector optical length) as a function of bulk lifetime and bias voltage. For long lifetime and low bias, the two-dimensional result is considerably higher, mainly because the excess carriers diffuse below the contacts and their concentration is not forced to zero at all depths. This is an effect similar to that of the overlap structure,[6] suggested for enhanced responsivity. At higher bias voltage the ratio is reduced, but the contribution of carriers flowing under the collecting electrode is present even under sweepout conditions. This result is verified by applying the analysis method of Williams[7] to the two-dimensional flow lines (assuming diffusion is negligible relative to drift). For very short bulk lifetimes, the two-dimensional responsivity is lower than the one-dimensional result, since excess carriers recombine before diffusing or drifting far from their generation site, and the average electric field in the two-dimensional device is lower than V/L.

Figure 5 shows the effect of varying the bias voltage on excess carrier distribution in a device which has a built-in retarding field for minority carriers near the collecting contact. Such a built-in field is caused by high donor concentration near the contact. This is

possible in HgCdTe by diffusion of indium atoms from the contact metallization.[13] It has been predicted on the basis of one-dimensional theory[2,3] that responsivity of such devices should not saturate at high fields, since excess carriers accumulate at the potential barrier instead of recombining at the contact. In practice, detectors with blocking contacts exhibit sweepout in their characteristics of responsivity vs bias, reaching values which are several times larger than predicted by the Rittner responsivity formula.[1] A one-dimensional model with partial blocking has been proposed to explain the experimental results,[10] assuming low blocking efficiency to obtain a fit. The cause for two-dimensional responsivity sweepout saturation, even with ideal blocking contacts, is illustrated in Fig. 5. It is seen that excess carriers are pushed towards the contact and diffuse laterally below the electrode, in a region where the field approaches zero. Thus, the contribution of these carriers to the integral in equation (8) is not significant, and the

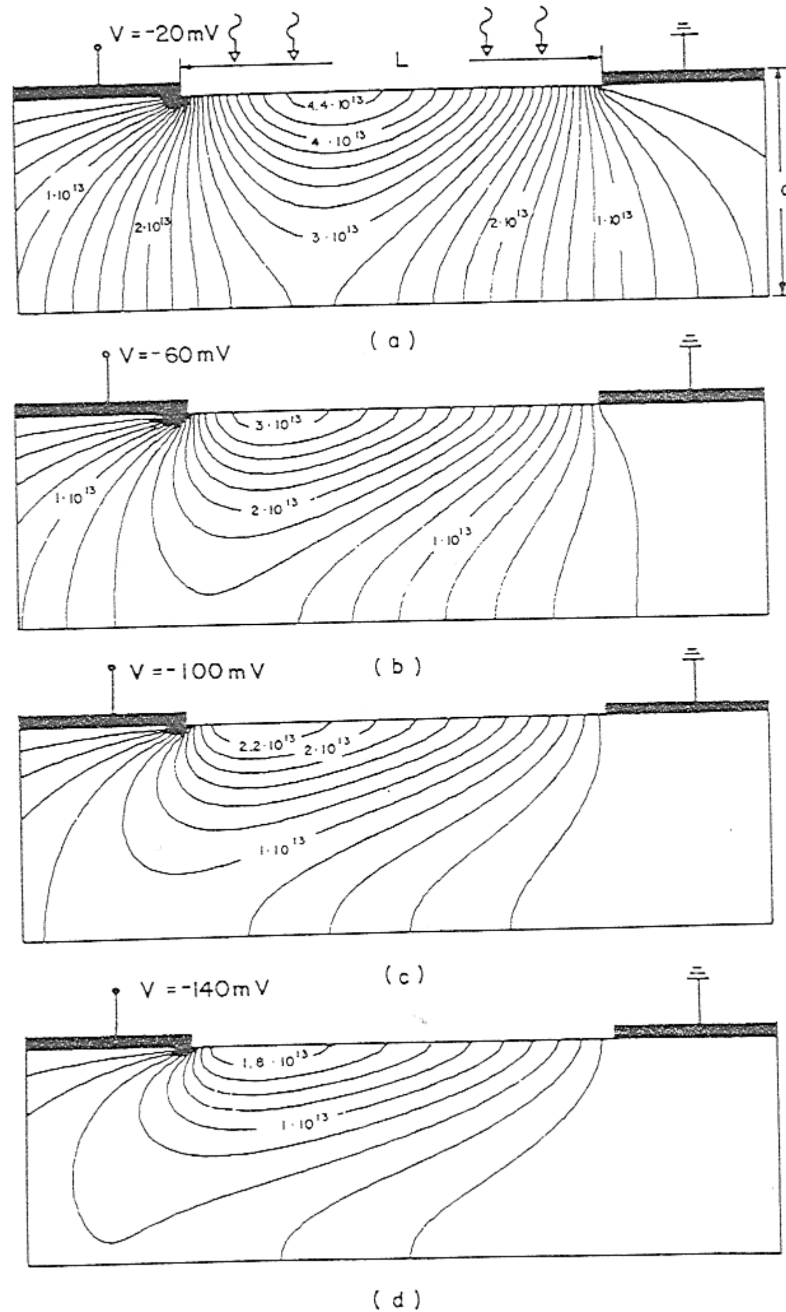

Fig. 3. Distributors of the excess carrier density in a photoconductor, with planar non-blocking contacts, for a few bias voltages. Sweepout to the negative contact shifts the distribution to the left and reduces the total amount of excess carriers. The simulations corresponds to n-type $Hg_{0.795}Cd_{0.205}Te$ at 77K, illuminated uniformly by a photon flux density of 10^{17} $cm^{-2}\cdot s^{-1}$ at 10 μm wavelength. $L = 28$ μm, $d = 15$ μm, $\tau_p = 10^{-6}$ s, $s = 0$ $cm\cdot s^{-1}$, $\mu_p = 500$ $cm^2\cdot V^{-1}\cdot s^{-1}$.

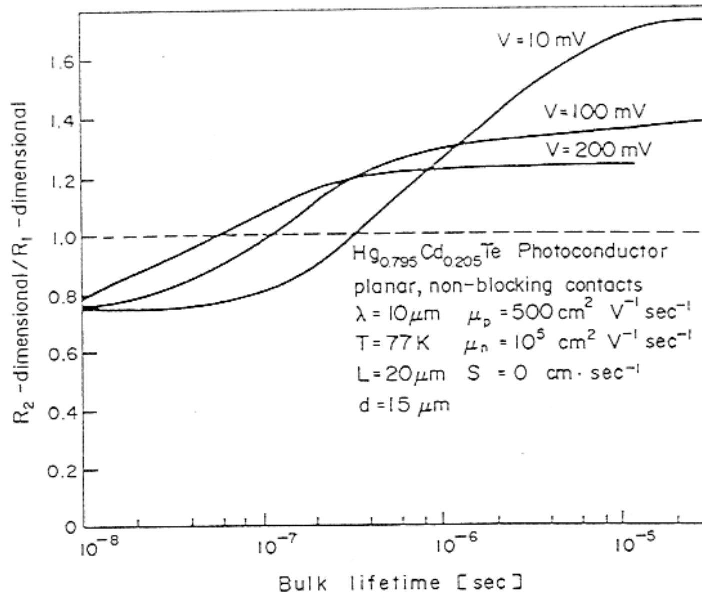

Fig. 4. Ratio of responsiveness calculated by two-dimensional and one-dimensional models for a planar-contact photoconductor, vs bulk lifetime. Three bias voltages are used in order to demonstrate sweepout effects.

responsivity does not increase linearly with increasing bias. Figure 6 shows experimental results on a $Hg_{0.795}Cd_{0.205}Te$ detector with blocking contacts, along with theoretical curves calculated for a few combinations of parameters. The standard one-dimensional non-blocking theoretical curve is also shown for reference. A perfect fit could not be obtained, mainly due to field-dependent mobility of the electrons which causes a decrease in device responsivity at high electric fields.[10]

The speed of response is a parameter of major importance in high-bandwidth systems using serial scene scan. Detectors are usually driven to high bias levels in order to achieve fast response. It was experimentally observed that response time in small devices is significantly slower than that predicted by one-dimensional theory, even when non-blocking contacts are used. The speed of response deviates from the simple theory as the device length is scaled down, since two-dimensional effects become important. An analysis of frequency response in a two-dimensional structure by solving equation (10) with a complex (phasor) excitation term is possible,[14] although excessive computation would be required. We suggest an approximate approach to derive an effective response time from the steady state responsivity. For a one-dimensional device, an effective lifetime is defined as

$$\tau_{eff} = \frac{\hat{P}}{\phi \cdot L} = \frac{\text{total excess carriers}}{\text{total generation rate}}. \tag{14}$$

Limiting expressions for τ_{eff} are τ_p, $(L/2)^2/3D_p$ and $L^2/2\mu_p V$, for the cases of recombination-dominated, diffusion-dominated and sweepout-dominated devices, respectively. The corresponding response times ($1/\omega_{3dB}$ calculated for these cases) are τ_p, $(L/2)^2/2.43D_p$ and $L^2/3.48\mu_p V$.[15] Therefore, it is reasonable to define an effective lifetime based on steady-state responsivity in a two-dimensional structure [equation (8)]. Hence,

$$\tau_{eff} = \frac{\displaystyle\iint \frac{\hat{p}(x, y)\,|E_0(x, y)|}{l(x, y)}\,\mathrm{d}x\,\mathrm{d}y}{\displaystyle(\phi \cdot L)\iint \frac{|E_0(x, y)|}{l(x, y)}\,\mathrm{d}x\,\mathrm{d}y} \tag{15}$$

which reduces to equation (14) if E_0 is constant and $l = L$ for all points (x, y) in the device. Figure 7 shows measured response times of an HgCdTe detector versus bias,

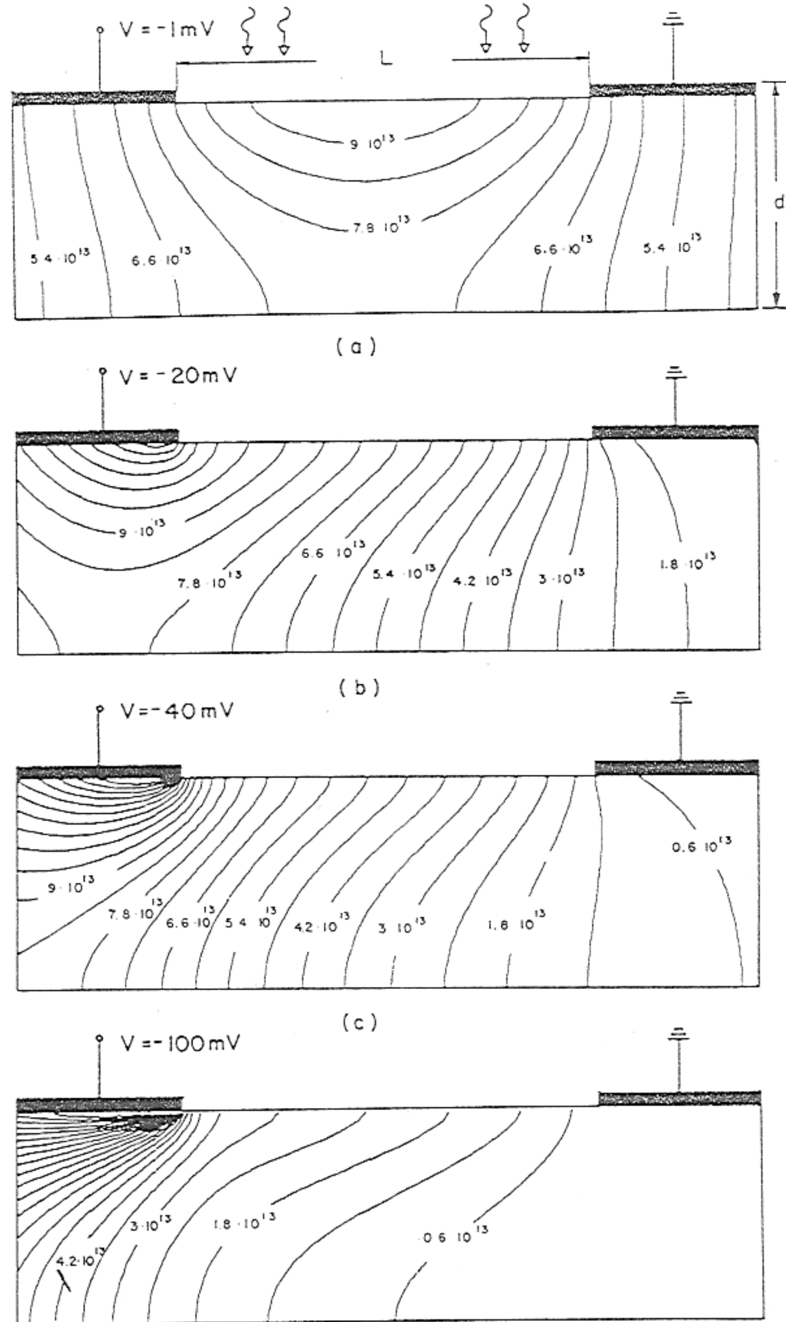

Fig. 5. Distribution of excess carriers in a photoconductor with blocking contacts, for a few bias voltages. At high fields the carriers are swept out of the active area and accumulate in the low-field region below the blocking contact, where their contribution to photoconductivity is minimal. This causes saturation in responsivity.

derived from the responsivity to a sine-wave modulated CO_2 laser beam. The figure shows in addition response time as derived from noise spectral measurements.[16] The figure also shows calculated response times using equation (15) and a one-dimensional frequency-domain solution. It is seen that a qualitative agreement is obtained with equation (15).

PHOTOCONDUCTORS WITH ASYMMETRIC CONTACTS

Photoconductive detectors are usually made in the form of linear arrays. Each sensitive element area is a rectangle defined by planar electrodes on two opposite sides. Separation between adjacent elements is achieved by removal of the semiconductor material. A novel mode for the realization of linear arrays of photoconductors is shown in Fig. 8. Here the elements are separated by a narrow metallization strip deposited upon the continuous semiconductor strip, forming a non-blocking common contact. In this

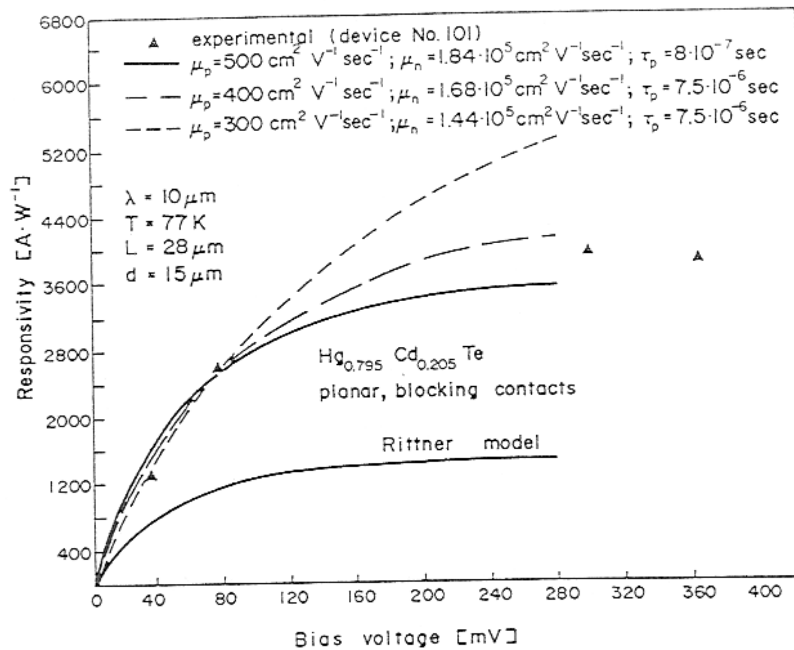

Fig. 6. Experimental results and simulated responsivity for a photoconductor with blocking contacts. The experimental device exhibits a decrease in responsivity at high fields due to scattering limited velocity of the electrons.

configuration more efficient use is made of the sensitive area on the array axis, in addition to the technological advantage gained in processing (no removal of the semiconductor material between elements is necessary). Due to the gross asymmetry in the form of the two electrodes to each element, the device is clearly two-dimensional with respect to the position of illumination. The response to a narrow beam of photons depends on the coordinate of impinging photons on the sensitive area. However, this is tolerable when the optical spot is of dimensions similar to the element area. In the following analysis we assume uniform absorption in the depth of the semiconducting film, and concentrate on two-dimensional effects in the x–y focal plane (Fig. 9a).

Figure 9b shows the calculated flow lines in the active region of a single array element. The electric field, is maximal near the small electrode, and approaches zero at the corners of the common electrode. Figures 9c and d depict excess carrier distributions in response to uniform illumination. In Fig. 9c the small electrode is positively biased, causing

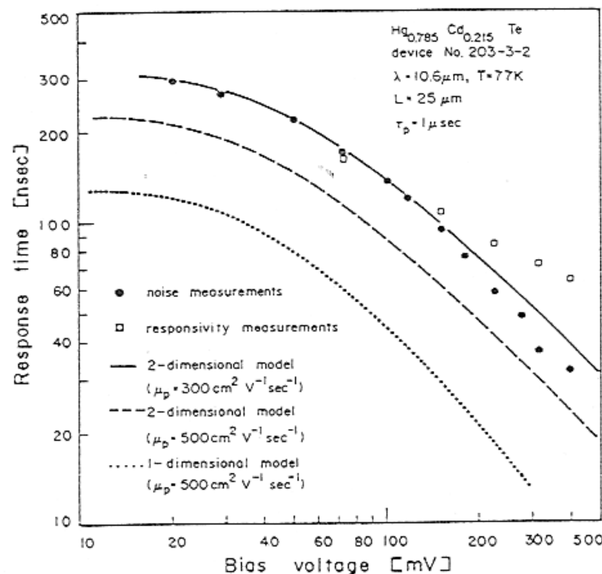

Fig. 7. Effective response time measured from responsivity and noise spectra, and calculated by two-dimensional and one-dimensional models.

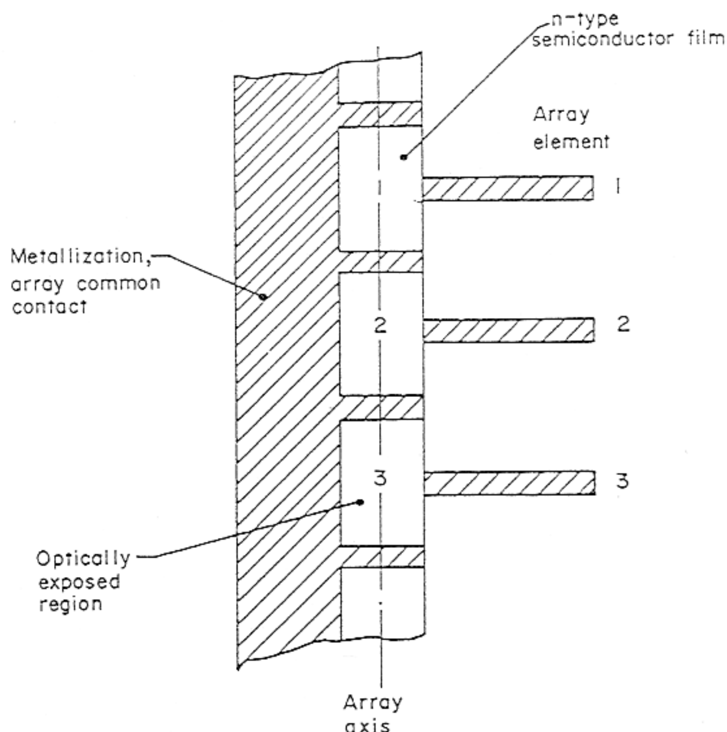

Fig. 8. A novel structure for a linear array of photoconductive detectors. Separation between elements is achieved by metallization rather than by removal of semiconductor material.

sweepout of the minority holes towards the periphery of the detector. In Fig. 9d this electrode is negatively biased, causing a pile-up of excess carriers in the middle. The total amount of excess carriers is higher in Fig. 9d since they are swept away from the recombining boundary at the large common electrode. In addition, the excess carriers are

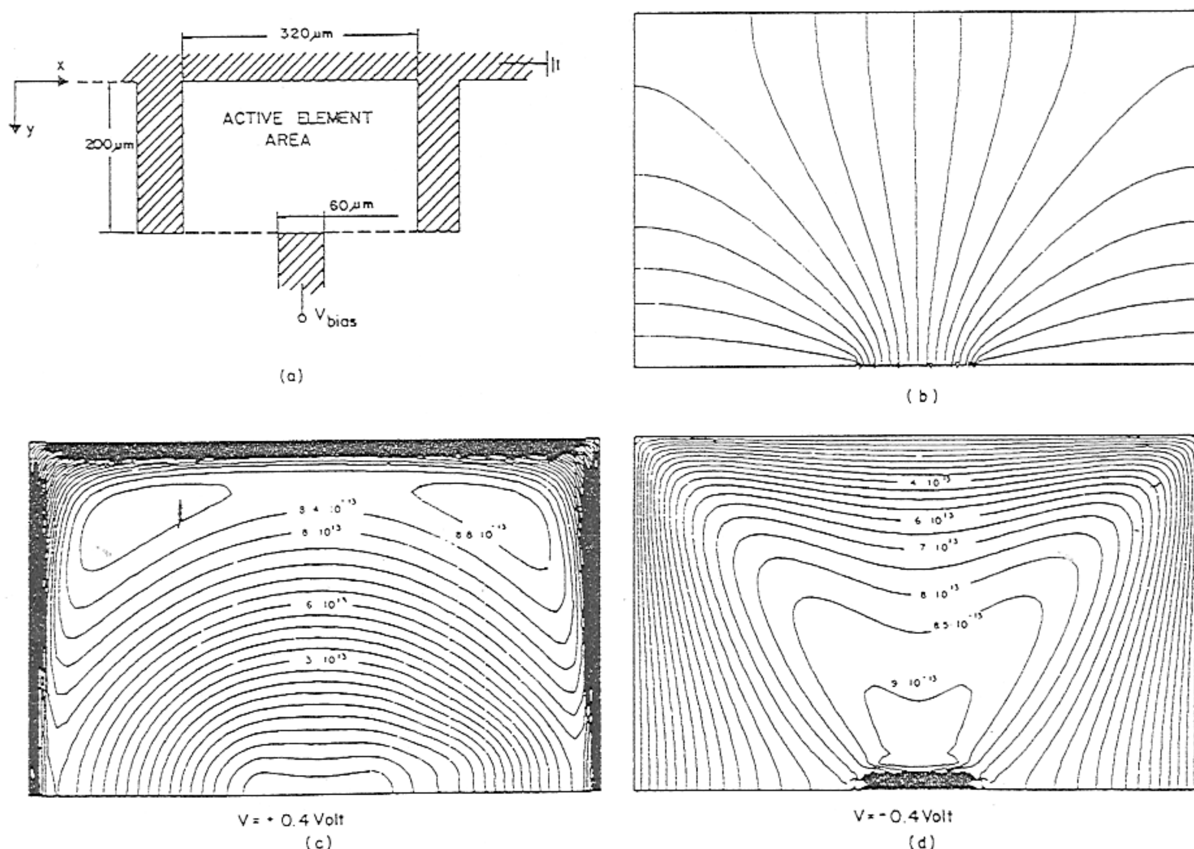

Fig. 9. (a) Top view of an array-element with asymmetric contacts. (b) Flow lines in the device. (c) Excess carrier density distribution (in cm^{-3}) under uniform illumination, for $V_{bias} = +0.4$ Volt, $\mu_p = 500\ cm^2 \cdot V^{-1} \cdot s^{-1}$, $\tau_p = 10^{-6}$ s, $\phi = 10^{17}\ cm^{-2} \cdot s^{-1}$, $d = 15\ \mu m$. (d) Excess carrier density distribution for the same parameters and negative bias polarity.

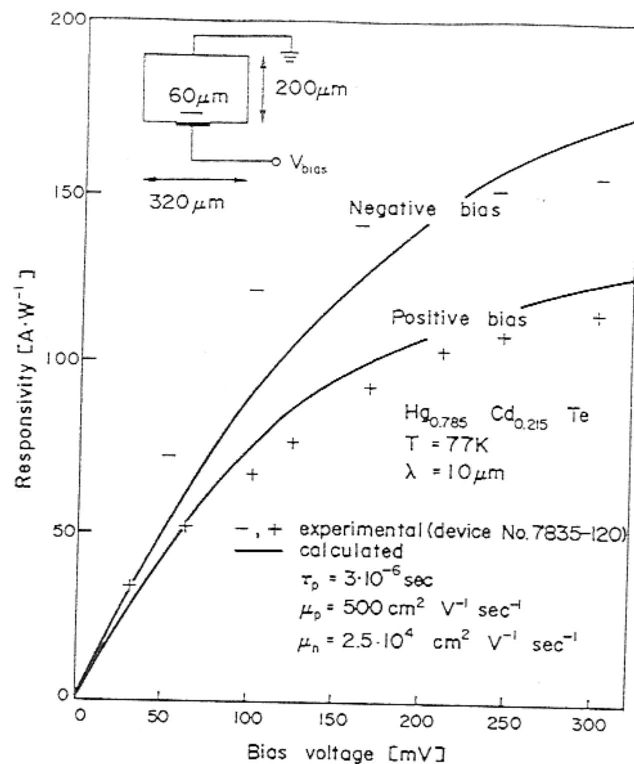

Fig. 10. Experimental and calculated responsivity of a photoconductor with asymmetric electrodes vs bias of both polarities. The device is *n*-type $Hg_{0.795}Cd_{0.215}Te$ at 77K, uniformly illuminated at 10 μm wavelength.

gathered in a region where the field intensity is high, while for positive bias (Fig. 9c) their maximum occurs at the low-field corners. Thus, the responsivity integral of equation (8) is larger for negative bias. Numerical and experimental results are shown in Fig. 10. In general, the smaller electrode should be negative for higher responsivity in any asymmetric structure.

The dependence of the detector sensitivity on the coordinates of illumination for the asymmetric device has been calculated by simulating a photon-beam of 40 μm dia. centered at 12 different points, as shown in Fig. 11a. Excess carrier distributions for illumination at two of these points are shown in Fig. 12, for both bias polarities. The calculated responsivity at each point is tabulated in Fig. 11b for a few bias voltages. As illustrated, sensitivity variations are affected by the non-uniform electric field, by diffusion to the recombining contacts, and by sweepout to the contacts. At very low bias, the spatial sensitivity map is similar to the field distribution. Diffusion to the contacts reduces the responsivity in the proximity of metallized periphery. For large positive bias, responsivity at any point should be proportional to the flow-distance from that point to the common electrode.[7,17,18] At negative bias, sweepout compensates the effects of contact-recombination and field-nonuniformity. Photocarriers generated near the common electrode and the low-field corners, are swept into the central region where their contribution to photoconductivity is enhanced. Excess carriers generated in the high-field region near the small electrode are swept out and their contribution is lowered. Therefore, negative bias is preferable in terms of both average responsivity and MTF uniformity.

To reduce crosstalk between adjacent elements the common array electrode should be non-blocking for minority carriers. In addition, the array elements should preferably be operated in the short-circuit mode, i.e. coupled to transfer resistance amplifiers. Finally, the recommended negative bias polarity is also effective in reducing crosstalk.

SUMMARY

A two-dimensional analysis of photoconductive detectors has been presented. We have shown that two-dimensional effects are significant in small-geometry photoconductive

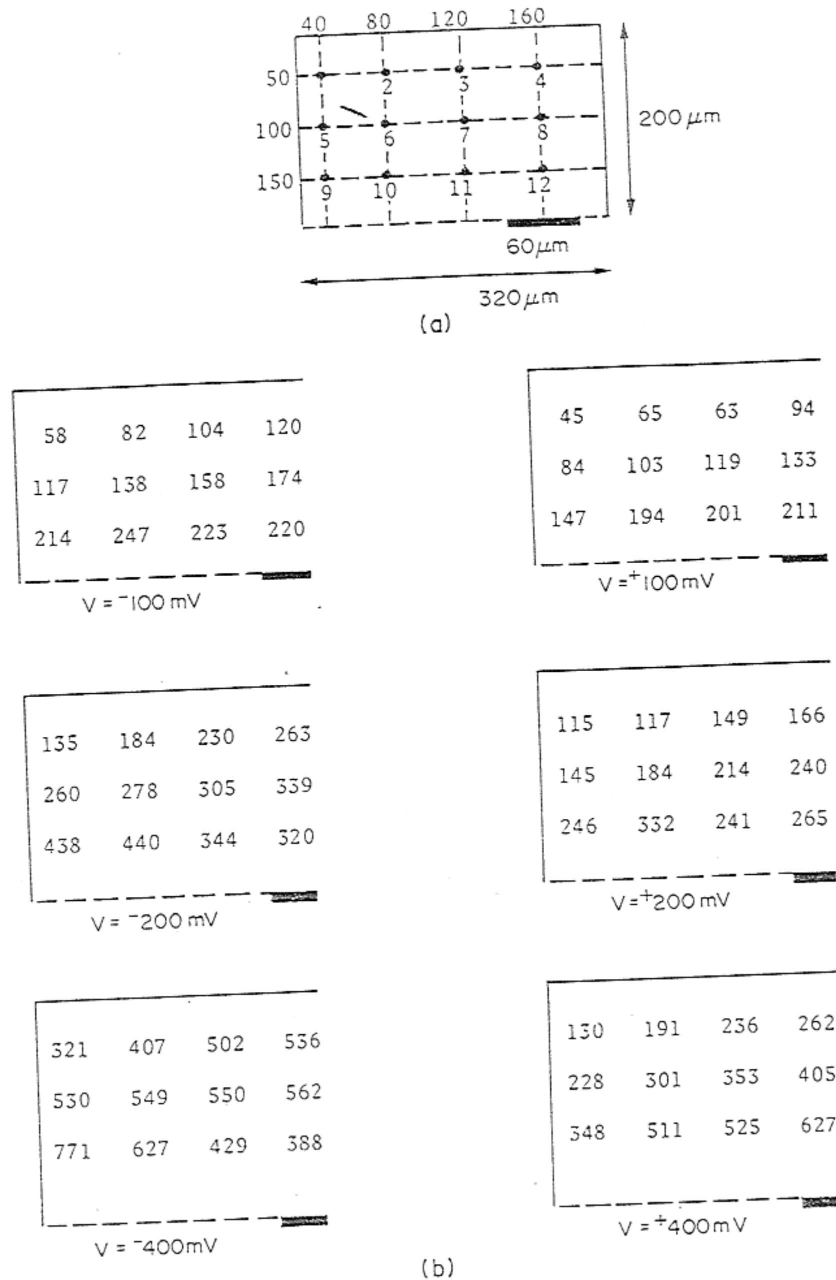

Fig. 11. (a) Definition of 12 points for responsivity calculation for device shown in Fig. 9a. (b) Tables of calculated responsivity at the 12 points shown in (a), for a few bias voltages. The results are in $A \cdot W^{-1}$ for a 40 μm dia. 10 μm wavelength photon beam centered at the point.

detectors. For planar-contact detectors with no blocking of minority-carriers at the electrodes, the two-dimensional effects on the detector responsivity are appreciable. Furthermore, the speed of response of such detectors, a parameter of particular importance, is significantly slower than predicted from one-dimensional theory. For design purposes the response time may be approximated by simple expressions, using an effective flow-length which is larger than the optically exposed length. Note that the transit-time is inversely proportional to the square of the effective flow length for a given bias voltage. In a planar-contact device, with minority carrier blocking at the electrodes, high responsivity is achievable at the expense of slower response. However, responsivity saturation occurs at high electric field due to sweeping of excess carriers out of the region contributing to photoconductivity. Although recombination takes place only in bulk material, the response time is appreciably shorter than the bulk lifetime due to this sweepout, and high bias is used in order to speed-up the response. For a given practical device it is not easy to distinguish between partial blocking and two-dimensional effects, since both lead to the same phenomena.[10]

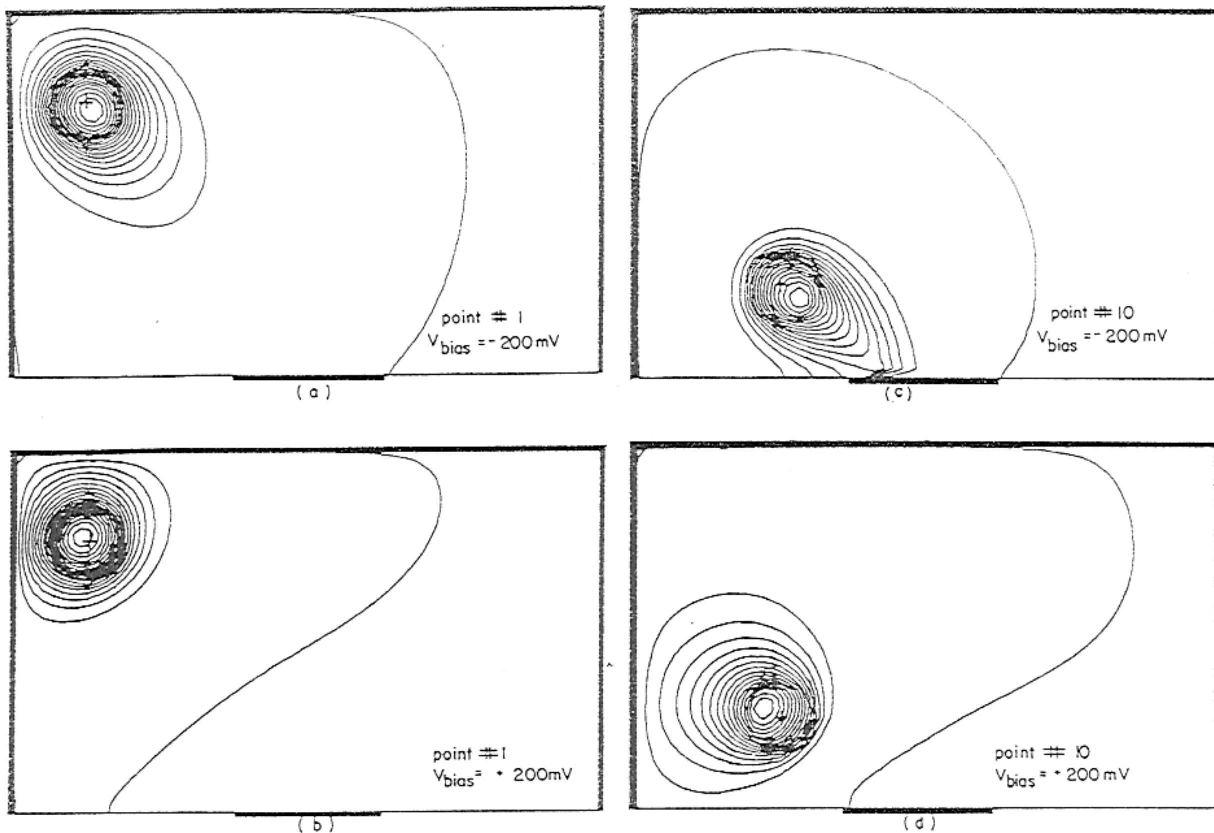

Fig. 12. Excess carrier distributions for illumination by a 40 μm dia. beam. (a) At point No. 1 (see Fig. 11) with negative bias. (b) At the same point with opposite bias polarity. (c) At point No. 10 with negative bias. (d) At the same point with opposite bias polarity.

A linear array structure has been proposed, which does not require removal of semiconductor material in order to separate adjacent elements. This structure is more convenient for processing, since it relaxes a technological constraint on the thickness of the semiconductor layer. As the thickness may be increased to some extent, it is possible to retain the original bulk lifetime (which is usually degraded in thinned layers), and minimize the detrimental effects of recombination at the rear surface. The sensitivity of each element with respect to position of illumination has been calculated for the asymmetric element geometry. When the minimum optical spotsize matches the element size, only the integrated responsivity over the sensitive area is important. Negative bias should be applied to the smaller electrode of the asymmetric device.

Acknowledgements—We are much indebted to Professor S. Margalit for his contribution to the asymmetric photoconductor and to I. Rotstein for his invaluable assistance in device processing.

REFERENCES

1. Rittner E. S., In *Photoconductivity Conference* (Edited by Breckenridge R. G.) Wiley, Atlantic City, New York (1956).
2. Long D., In *Topics in Applied Physics*, Vol. 19, *Optical and Infrared Detectors* (Edited by Keyes R. J.). Springer-Verlag, Berlin (1977).
3. Rose A., *Interscience Tracts in Physics and Astronomy*, No. 19. Wiley, New York (1963).
4. DeVore H. B., *Phys. Rev.* **102**, 86 (1956).
5. Kinch M. A., S. R. Borello & A. Simmons, *Infrared Phys.* **17**, 127–135 (1977).
6. Kinch M. A., S. R. Borello, B. H. Breazeale & A. Simmons, *Infrared Phys.* **17**, 137–145 (1977).
7. Williams R. L., *Infrared Phys.* **8**, 337–343 (1968).
8. Pines M. Y. & R. H. Genoud, *Proc. IEDM*, Washington, D.C., p. 456 (1976).
9. van Vliet K. M., *Appl. Opt.* **6**, 1145–1169 (1967).
10. Shacham-Diamand Y. J. & I. Kidron, *Infrared Phys.* **21**, 105–115 (1981).
11. McKelvey J. P., *Solid-State and Semiconductor Physics*, p. 320, Harper & Row, 1966.
12. Many A., Goldstein Y. & Grover N. B., *Semiconductor Surfaces*. North-Holland, Amsterdam (1965).
13. Margalit S. & Nemirovsky Y., *J. Electrochem. Soc.* **127**, 1406 (1980).

14. SELTZ D. & KIDRON I., *IEEE Trans. on Electron Devices*, **ED-21**, 587–592 (1974).
15. SHACHAM-DIAMAND Y. J., private communication.
16. MAZURCZYK U. J., GRANEY R. N. & MCCULLOUGH J. B., *Opt. Eng.* **13**, 307, (1974).
17. EMMONS S. P. & ASHLEY K. L., *App. Phys. Lett.* **20**, 162 (1972).
18. JOHNSON M. R., *J. Appl. Phys.* **43**, 3090 (1972).